Radial Peripapillary Capillary Plexus Sparing and Underlying Retinal Vascular Impairment in Intermediate Age-Related Macular Degeneration

Matt Trinh,[1,2] Michael Kalloniatis,[1,2] and Lisa Nivison-Smith[1,2]

[1]Centre for Eye Health, University of New South Wales, Sydney, Australia
[2]School of Optometry and Vision Science, University of New South Wales, Sydney, Australia

Correspondence: Lisa Nivison-Smith, School of Optometry and Vision Science, University of New South Wales Australia, Rupert Myers Bldg, Gate 14, Barker St, Sydney, 2052, NSW, Australia; l.nivison-smith@unsw.edu.au.

Received: December 21, 2020
Accepted: March 6, 2021
Published: April 1, 2021

Citation: Trinh M, Kalloniatis M, Nivison-Smith L. Radial peripapillary capillary plexus sparing and underlying retinal vascular impairment in intermediate age-related macular degeneration. *Invest Ophthalmol Vis Sci.* 2021;62(4):2. https://doi.org/10.1167/iovs.62.4.2

Purpose. To examine location-specific retinal vascular changes in intermediate age-related macular degeneration (iAMD) using age-matched, high-density en face optical coherence tomography angiography (OCTA) cluster analysis.

Methods. En face OCTA images of the 6 × 6 mm macular area were retrospectively acquired from 60 iAMD eyes and 60 age-matched normal eyes and then subdivided into 126 × 126 (47.62 × 47.62 µm) grids within the superficial and deep vascular complex. Grid-wise vessel perfusion (VP) were compared between iAMD and normal eyes from the corresponding 10-yearly age cohort, forming difference plots. Difference plots were further separated by normative topographical map spatial clusters ($C_{1\text{-}6}$), derived from $normal_{database}$ eyes (n = 236, 20–81 years old).

Results. Overall difference plots showed decreased VP in the superficial (−12.19%) and deep vascular complex (−6.44%) of iAMD compared to normal eyes ($P < 0.0001$ both comparisons). Cluster-based difference plots highlighted nonuniform changes in the superficial vascular complex, with sparing of VP at the nasal macula (corresponding to the radial peripapillary capillary plexus) versus decreased VP toward the temporal macula and foveal avascular zone (FAZ) (C_{1-6} all comparisons $P < 0.0001$, except C_1 vs. C_2 $P > 0.99$ and C_4 vs. C_5 $P = 0.11$). The deep vascular complex displayed diffusely decreased VP, greater at the FAZ ($P < 0.0001$).

Conclusions. High-density en face OCTA cluster analysis suggests relative sparing of the radial peripapillary capillary plexus and impairment of underlying retinal vasculature, supporting potential anterograde transsynaptic degeneration in iAMD. These location-specific data may better guide future diagnostic and management protocol of iAMD.

Keywords: optical coherence tomography angiography, vessel perfusion, age-related macular degeneration

Age-related macular degeneration (AMD) is one of the leading causes of irreversible blindness worldwide,[1] typically characterized by insult at the outer retina.[2] Studies using a variety of techniques such as histology and Doppler flowmetry have also implicated an expanse of vascular changes associated with the early stages of AMD, including decreased flow and increased resistivity of extraocular vessels,[3–7] and altered structure of intraocular vessels at the choroid and retina.[8–11] More recently, optical coherence tomography angiography (OCTA) studies have provided greater insight into in vivo intraocular vascular change associated with the early stages of AMD,[12–23] demonstrating new opportunities for clinical assessment of the disease.

OCTA studies describing retinal vascular change in the early stages of AMD demonstrate conflicting results. Some studies report reduced vessel density or perfusion in the superficial, deep or both vascular complexes,[12–17,19,24] whereas others describe no significant changes in either vascular complex.[18,20–23] Varying study designs such as lack of control or adjustment for signal strength (which has a significant effect on OCTA outcomes)[25–27] in a majority of OCTA studies may explain discordant results. Also of note, all studies[12–16,18–23] except Trinh et al.[17] have analyzed retinal vasculature within a 3 × 3 mm macular area, overlooking vascular change that may occur beyond this area. Meanwhile, a paucity of research into more localized retinal vascular changes in the early stages of AMD may also explain conflicting results. Studies that have provided further spatial analysis[13,14,18] were based on the early treatment for diabetic retinopathy study (ETDRS) sectors, which assume concentricity around the fovea, in discordance with actual retinal vascular topography, which emanates from a nasally situated optic nerve head.[28,29] The lack of appropriate spatial detail with regards to OCTA studies of the retinal vasculature means that there is a current gap in knowledge regarding where the retinal vasculature may be impacted in the early stages of AMD, which would be valuable to guide future diagnostic and management protocol.

Recently, in vivo topographical maps that follow histologically defined retinal topography have been developed

for both retinal structural and functional outcomes using a process known as "spatial clustering."[30–34] Clustering involves the grouping of data according to statistical likeness, facilitating reduced variability compared to non-cluster analyses because comparison of output parameters to a cluster of data is statistically more powerful than comparison to individual data.[34] However, OCTA output in the early stages of AMD are yet to be assessed using spatial clustering, potentially missing important spatial detail in the vascular pathophysiology of AMD. Thus this study applies high-density en face OCTA cluster analysis to examine location-specific retinal vessel perfusion (VP) changes of intermediate AMD (iAMD) eyes versus age-matched normal eyes. By elucidating the spatial patterns of retinal vascular change in the early stages of AMD, we may better understand its pathophysiology and provide guidance toward specific retinal areas of interest for future diagnostic and management protocols.

Methods

Study Population

Participant data were obtained through retrospective analysis of records from July 7, 2016, to June 5, 2020, of patients attending the Centre for Eye Health in Sydney, Australia. The Centre for Eye Health is a referral-only clinic providing advanced diagnostic eye testing and disease management by specially trained optometrists and ophthalmologists.[35] All patients had given prior written informed consent to use their deidentified data for research in accordance with the Declaration of Helsinki and approved by the Biomedical Human Research Ethics Advisory Panel of the University of New South Wales.

Inclusion criteria for normal eyes were no evidence of posterior ocular disease nor any significant structural abnormalities such as subretinal or intraretinal deposits, pigment, fluid, or vascular abnormalities within the 6 × 6 mm area surrounding the fovea. Studies have demonstrated minimal to no significant difference in results using a 3 × 3 mm or 6 × 6 mm image, although the latter provides a greater field of view.[36–39] Inclusion criteria for iAMD eyes were age 50 years or older, diagnosis of iAMD,[40] and no evidence of other posterior ocular disease nor significant structural abnormalities unrelated to iAMD within the 6 × 6 mm area surrounding the fovea. Classification of iAMD were based on evaluations of fundus photography between at least two nonblind investigators using a modified Beckman Initiative classification system,[40] that is, participants 50 to 54 years of age in this study were considered to have iAMD if they followed all iAMD phenotypic criteria in the classification system (as has been done in other notable studies).[41–44] Specifically, iAMD eyes had large drusen (>125 µm) or pigmentary abnormalities associated with at least medium drusen (63–125 µm), without signs of late AMD such as neovascularization, geographic atrophy, or both. Scanning laser ophthalmoscopy photography and OCTs (Cirrus SD-OCT ~21° × 21° macular volume scans; Carl Zeiss Meditec, Jena, Germany; Spectralis SD-OCT 30° × 25° macular volume scans; Heidelberg Engineering, Heidelberg, Germany) were used to exclude eyes with signs of late AMD or other posterior ocular disease. Any participants with hypertension, diabetes mellitus, or other significant systemic vascular disease that may confound OCTA outcomes were excluded from analyses.[45–48]

Image Acquisition

Cirrus HD-OCT v11.0.0.29946 Zeiss Cirrus Angioplex (Carl Zeiss Meditec; Jena, Germany) 6 × 6 mm (20.93° × 20.93°) en face macular cube scans were extracted for the superficial and deep retinal vascular slabs.[17] Only one eye per participant was included in this study. In cases where both eyes of a participant were eligible for inclusion, the image with higher signal strength index (SSI) and lesser artefacts were selected. Scans were accompanied by fixation-tracking software, a motion correction algorithm, and a projection removal tool. Retinal vascular slabs were automatically segmented based on the Zeiss Cirrus Angioplex definitions of the superficial vascular slab (between the inner limiting membrane to approximately the outer border of the inner plexiform layer; also known approximately as the superficial vascular complex; Supplementary Fig. S1A)[29] and the deep vascular slab (between approximately the outer border of the inner plexiform layer to approximately the outer border of the outer plexiform layer; also known approximately as the deep vascular complex; Supplementary Fig. S1B).[29] Any images with significant segmentation errors that were not manually correctable by MT or LNS were excluded, that is, one image. Images with missing B-scans, significant artefacts (e.g., blinking or motion artefacts), or SSI less than seven were excluded.

Postimage Processing

Postimage processing using ImageJ v1.52a (National Institutes of Health, Bethesda, MD, USA) involved 8-bit conversion of en face OCTA images of the superficial and deep vascular complex, binarization (using the auto-threshold default method because of its proven reliability and diagnostic sensitivity and specificity),[49] and skeletonization whereby all vessels were converted to a single pixel width (5.95 µm or 0.02°).[17] Images were then divided into 126 × 126 equal grids (47.62 × 47.62 µm or 0.17 × 0.17°) using "stacks," and grid-wise VP quantified as the percentage of pixels attributing to a vascular flow signal per grid (Fig. 1A). VP were used rather than vessel density to eliminate the potential confounding effect of vessel diameter (i.e., changes in vessel density may be related to vessel diameter, length, or both, whereas changes in VP are only related to vessel length because of skeletonization). VP has also been shown to be more sensitive to perfusion changes than vessel density.[50]

Development of Normative Topographical Maps of VP in the Superficial and Deep Vascular Complex

Normative OCTA-derived topographical maps of VP in the superficial and deep vascular complex were derived using a process analogous to what has been previously done for OCT-derived normative topographical maps of retinal layer thicknesses.[31,32,34] Specifically, en face OCTA images from a large database of $\text{normal}_{\text{database}}$ eyes of varying ages (n = 236 eyes from 236 participants, 20–81 years old; Supplementary Table S1) were acquired and processed into 126 × 126 equal grids, with each grid VP quantified as described above. Considering the covariables of age, SSI, right or left eye, sex, ethnicity, spherical equivalent refraction, ganglion cell complex thickness, retinal nerve fiber layer thickness, and ganglion cell layer-inner plexiform layer thickness versus average VP in multi-variable regression, age (as expected) were the only covariables significantly associated with

Investigative Ophthalmology & Visual Science

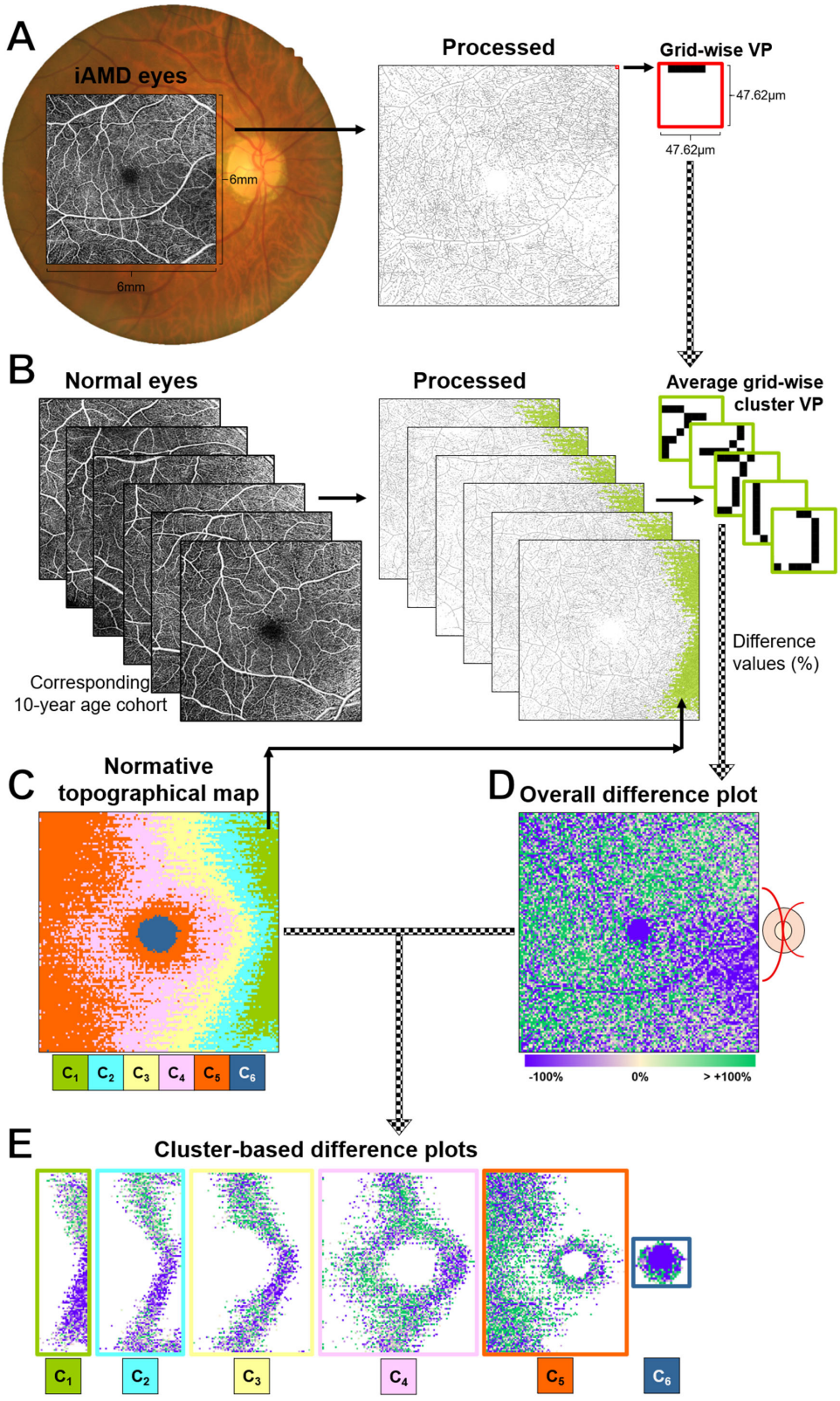

Figure 1. Schematic example of age-matched, high-density en face OCTA cluster analysis of the superficial vascular complex for a 63-year old Asian male with iAMD. **(A)** 6 × 6 mm en face OCTA image were extracted and processed (8-bit, binarized, and skeletonized), then divided into 126 × 126 (15,876) equal grids (47.62 × 47.62µm). Underlying fundus photo provided for spatial context. Grid-wise VP were quantified (*red square*). **(B)** The same process was applied to normal eyes from the corresponding 10-yearly age cohort of 60-69 years old. Average grid-wise cluster VP were quantified (*green squares*), whereby spatial clusters were derived from the normative topographical maps of VP

Investigative Ophthalmology & Visual Science

in the superficial vascular complex (represented by distinct colors) **(C)**. Grid-wise VP were subtracted by the average grid-wise cluster VP of normal eyes from the corresponding 10-year age cohort and displayed as a percentage of the latter, forming percentage difference values (*checkered arrows*). Percentage difference values were assigned a color scale, and calculation for all 15,876 grids resulted in a qualitative and quantitative **(D)** overall difference plot. The overall difference plot was further separated according to the aforementioned clusters (C), forming **(E)** cluster-based difference plots. Analyses were repeated in the deep vascular complex. All images are in right eye format as demonstrated by the optic nerve location. OCTA, optical coherence tomography angiography; VP, vessel perfusion; iAMD, intermediate age-related macular degeneration; $C_{1\text{-}6}$, cluster 1−6 in order of highest to lowest VP.

average VP in the superficial and deep vascular complex that were not equally distributed between $normal_{database}$ 10-yearly age cohorts ($\beta = -0.01$, $P < 0.0001$ for both complexes; Supplementary Table S2).

Average grid-wise VP for each 10-yearly age interval in each retinal vascular complex were then grouped into spatial clusters of statistically similar values using K-means clustering via SPSS Statistics v25.0 (IBM Corporation, Armonk, NY, USA).[31,32,34] This method was selected because of its proven robustness against other traditional clustering methods.[51] For each retinal vascular complex across all age groups, final cluster numbers were selected on the basis of the maximum number of clusters required to separate cluster means by ≥1 SD (equivalent to $d' = 1$ from signal detection theory).[52] Cluster separability were confirmed using Tukey's multiple comparisons test for the superficial vascular complex and Student's *t*-test for the deep vascular complex ($P < 0.0001$ all comparisons). Resultant clusters formed normative topographical maps of VP in the superficial and deep vascular complex, useful as a spatial template for further location-specific analysis of iAMD eyes.

Location-Specific Analysis of iAMD Eyes Compared to Age-Matched Normal Eyes

Grid-wise VP of iAMD eyes (Fig. 1A) were subtracted by the average grid-wise cluster VP of normal eyes from the corresponding 10-year age cohort (Fig. 1B), whereby spatial clusters were derived from normative topographical maps of VP in both the superficial (Fig. 1C) and deep vascular complex. Resultant difference values were displayed as a percentage of the average grid-wise cluster VP of normal eyes, whereby negative values indicated decreased VP, and positive values indicated increased VP in iAMD eyes. Percentage difference values were assigned a color scale, and calculation for all 15,876 grids formed qualitative and quantitative overall difference plots (Fig. 1D). Overall difference plots were further separated by the aforementioned clusters that formed the normative topographical maps, creating cluster-based difference plots (Fig. 1E). The process is summarized in Figure 1 (checkered arrows).

Mitigating the effect of skewed data as comparison to normative values near zero would elicit a greater percentage magnitude of difference than comparison to normative values near 100%, and the median difference (%) was used as the primary summary statistic.

Comparison of Location-Specific Analysis Using Clusters Versus Traditional Methods

Location-specific analysis using clusters to define the normative topography of VP were also compared to traditional definitions of normative topography. The same processes as above were applied to form overall difference plots comparing grid-wise VP of iAMD eyes to average grid-wise VP of a global area or average grid-wise VP of ETDRS sectors (using grids matching the sectors as closely as possible) of normal eyes. Comparisons were then drawn between the various methods, that is, using clusters versus a global area versus ETDRS sectors.

Statistical Analysis

Statistical analyses were performed using GraphPad Prism Version 8, SPSS Version 25, and Microsoft Excel Version 2009. Significance was considered as $P < 0.05$. Multivariable linear regression using backward stepwise elimination[53] was performed to determine potential confounders associated with VP. Single comparisons between continuous variables

Table. Normal and iAMD Participant Demographics

	Normal	Intermediate AMD	*P* Value
Eyes, n			
Total	60	60	—
50-69	17	11	
60-69	27	24	0.18*
70+	16	25	
Age (years)			
Total	65.26 ± 6.87	67.32 ± 8.2	0.14†
50-69	57.13 ± 1.97	55.92 ± 2.87	0.2‡
60-69	65.18 ± 3.07	64.09 ± 2.95	0.2‡
70+	74.01 ± 2.96	75.45 ± 3.81	0.23‡
Sex (males/females)			
Total	26:34	21:39	0.45§
50-69	12:5	9:2	0.67§
60-69	13:14	14:10	0.58§
70+	9:7	16:9	0.75§
Ethnicity (W:A:O)			
Total	31:13:16	35:7:18	0.34*
50-69	6:4:7	6:2:3	0.6*
60-69	15:7:5	12:4:8	0.43*
70+	10:2:4	17:1:7	0.59*
SE Rx (diopters)			
Total	0.41 ± 1.43	0.43 ± 1.95	0.95†
50-69	-0.02 ± 1.38	0.61 ± 0.61	0.22‡
60-69	0.46 ± 1.35	0.27 ± 2.01	0.17‡
70+	0.77 ± 1.56	0.53 ± 2.25	0.78‡
SSI			
Total	9.43 ± 0.77	9.17 ± 0.96	0.1†
50-69	9.18 ± 1.07	9.73 ± 0.47	0.21‡
60-69	9.56 ± 0.58	9 ± 1.08	0.1‡
70+	9.5 ± 0.63	9.12 ± 0.93	0.23‡

Continuous values are expressed as mean ± standard deviation (SD). Categorical values are expressed as counts. Cohorts were analysed by 10-yearly age intervals.

W, White; A, Asian; O, Other; SE Rx, spherical equivalent refraction; SSI, signal strength index.

* χ^2 test.

† Student's t-test

‡ Mann-Whitney *U* test

§‖ Fisher's exact test.

Investigative Ophthalmology & Visual Science

were assessed with the Student *t*-test or Mann-Whitney *U* test, depending on the relevant assumptions for data. Multiple comparisons were performed with Mann-Whitney *U* testing with the Bonferroni adjustment, that is, significance considered as $P < \frac{0.05}{6}$ for the superficial vascular complex clusters or $P < \frac{0.05}{2}$ for the deep vascular complex clusters, or Kruskal-Wallis and Dunn's multiple comparison tests where appropriate. Multiple comparisons of variance were performed using the Brown-Forsythe test.

Results

Participant Demographics

Sixty eyes with iAMD from 60 participants and 60 normal eyes from 60 age-matched participants were included in location-specific analysis. There was no significant difference with age, sex, ethnicity, spherical equivalent refraction, or SSI between the two cohorts (Table 1).

Location-Specific Analysis in the Superficial Vascular Complex

In the superficial vascular complex, $normal_{database}$ grid-wise VP were averaged across 10-yearly cohorts and grouped into spatial clusters based on statistically similar values across all age groups. The normative topographical map showed a temporal-to-nasal cluster pattern with a semblance of concentricity ($C_{1\text{-}6}$ in order of highest to lowest VP; Fig. 2A). Cluster means were confirmed to be significantly different (Tukey's multiple comparisons test, $P < 0.0001$ all comparisons).

Using this normative topographical map as a spatial template for further location-specific analysis, we formed a difference plot of iAMD eyes compared to normal eyes. The overall difference plot demonstrated significantly decreased VP (median difference, −12.19%, $P < 0.0001$; Fig. 2B).

The magnitude of these VP changes clearly varied with spatial location across the macula, and to further explore this, the overall difference plot was separated into clusters (Fig. 2C). There were no significant differences in VP at C_1 and C_2 (Mann-Whitney *U* tests; median difference, −0.4% and 0.62%, adjusted $P = 0.27$ and 0.03, respectively), but significant differences in VP at $C_{3\text{-}6}$ (−8.4%, −17.35%, −19.39%, and −100%, respectively; adjusted $P < 0.0001$ for all comparisons; Fig. 2D). Decreased VP in iAMD eyes were greater for clusters toward the temporal macula ($C_{4\text{–}5}$) and FAZ (C_6) (Kruskal Wallis test $P < 0.0001$, post-hoc Dunn's multiple comparisons test $P < 0.0001$ for all inter-cluster comparisons except C_1 vs. C_2 $P > 0.99$, and C_4 vs. C_5 $P = 0.11$).

Location-Specific Analysis in the Deep Vascular Complex

In the deep vascular complex, the normative topographical map showed a relatively diffuse pattern occupied largely by a single cluster (C_1) with a second smaller cluster at the FAZ (C_2, in order of highest to lowest VP; Fig. 3A). Cluster means were confirmed to be significantly different (Student's *t*-test, $P < 0.0001$).

When this normative topographical map was used for further location-specific analysis of iAMD eyes, the overall difference plot demonstrated significantly decreased VP for iAMD eyes compared to normal eyes (median difference, −6.44%, $P < 0.0001$; Fig. 3B). Decreased VP in the deep vascular complex were lesser in magnitude compared to the superficial vascular complex (−6.44% vs. −12.19%, respectively; $P < 0.0001$).

Further separation of the overall difference plot into clusters (Fig. 3C) showed significant differences in VP at C_1 and C_2 (−6.07% and −24.38%, respectively; adjusted $P < 0.0001$ for both comparisons; Fig. 3D). Decreased VP were greatest at the FAZ cluster (C_2 vs. C_1, $P < 0.0001$), whereas decreased VP at C_1 were mostly diffuse with subtly lesser magnitude toward the temporal area.

Correlation of Grid-Wise VP Between the Superficial and Deep Vascular Complex

There remained a possibility that outcomes in the deep vascular complex were shaped by outcomes in the superficial vascular complex, because the nature of en face imaging means that the penetration of OCTA signal to the deep vascular complex may be contingent on initial penetration through the superficial vascular complex. Therefore we correlated VP between the superficial and deep vascular complex for each normal and iAMD eye. We found no significant correlation for overall VP ($P = 0.69$ and 0.48, respectively).

Grid-wise VP between the superficial and deep vascular complex also showed no significant correlations in most areas and otherwise weak-to-moderate correlations in very limited areas. Specifically, most grids were either not significantly correlated ($P \geq 0.05$; 14,608/15,896 [91.9%] for normal eyes and 14,703 [92.49%] for iAMD eyes) or weakly correlated (Spearman's $r < 0.3$; $P < 0.05$; 454/15,896 [2.86%] for normal eyes and 458/15,896 [2.88%] for iAMD eyes; Fig. 4]. In a minority of grids, there were significant moderate correlations (Spearman's $r = 0.3$ to 0.6; $P < 0.05$ for *colored* grids; 834/15,896 [5.27%] grids for normal eyes and 735/15,896 [4.62%] grids for iAMD eyes). There was also a statistically significant but weak association between the strength of grid-wise correlation and cluster location in normal and iAMD eyes (Spearman's $r = 0.15$ and 0.08; $P < 0.0001$ and < 0.01, respectively), that is, correlation of grid-wise VP between the superficial and deep vascular complex were stronger toward the temporal macula and FAZ clusters. Qualitatively, this aligned with observations that correlations were stronger at the peripheral macula and perifovea, coinciding with areas where the vascular plexuses converge anatomically.

Comparison of Location-Specific Analysis Using Clusters Versus Traditional Methods

The performance of location-specific analysis using clusters was compared to traditional methods of using a global area or ETDRS sectors to define normative topography of VP. Overall difference plots of the superficial vascular complex using each method highlighted a similar pattern of decreased VP towards the temporal macula and FAZ (Figs. 5A–5C). Median difference VP were significantly less using clusters versus a global area versus ETDRS sectors, suggesting conservative outcomes using clusters or exaggerated outcomes using traditional methods (Kruskal Wallis test $P < 0.0001$; −12.19% vs. −15.81% vs. −15.18%, respectively; post-hoc Dunn's multiple comparisons test $P < 0.0001$

Investigative Ophthalmology & Visual Science

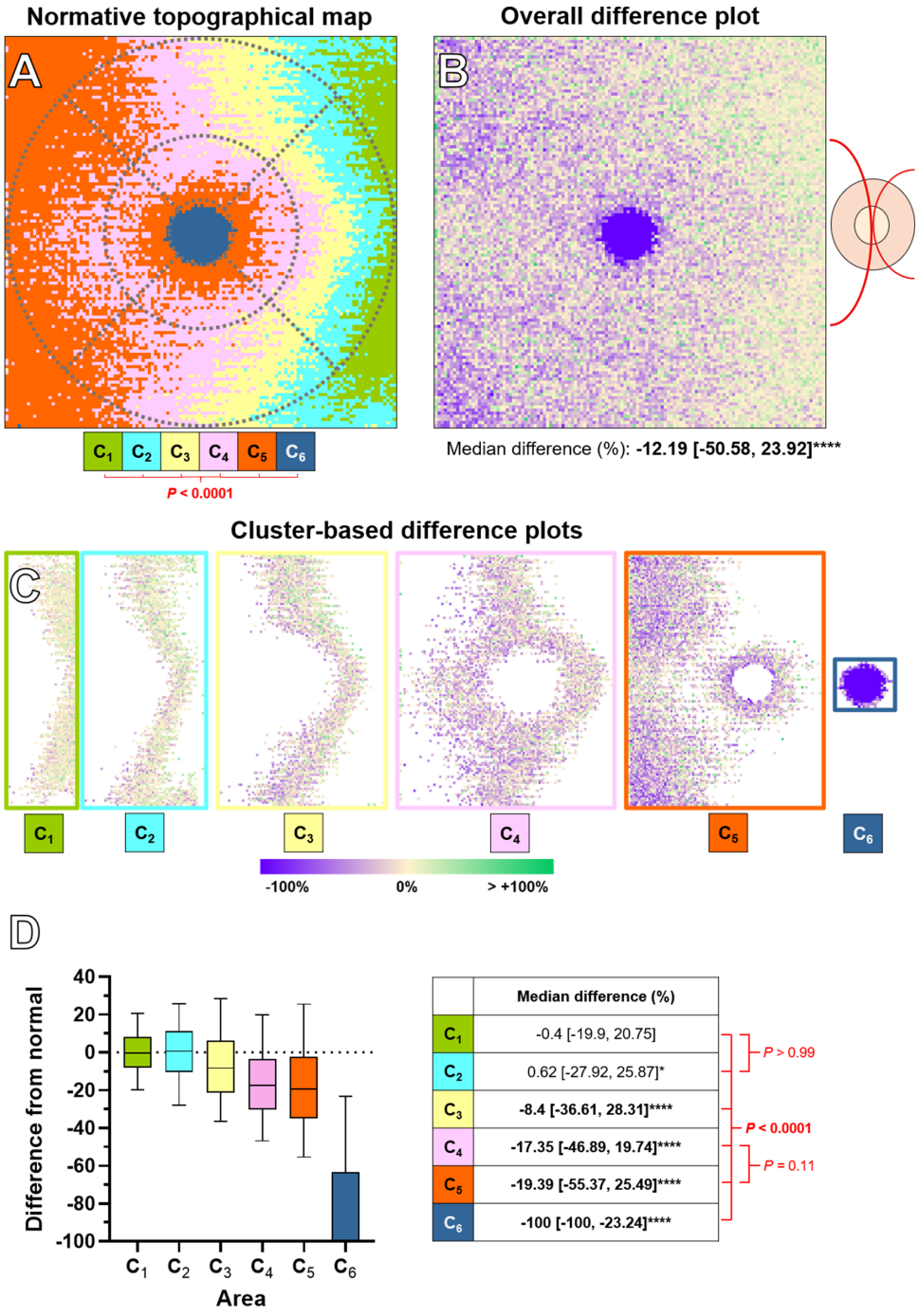

Figure 2. Location-specific analysis: VP difference plots of iAMD eyes compared to normal eyes for the superficial vascular complex. All images are in right eye format as demonstrated by the optic nerve location. **(A)** Normative topographical map of VP in the superficial vascular complex (*gray* ETDRS overlay for reference). Each cluster is represented by distinct colors and includes grid-wise locations of statistically similar values. Mean ± SD values in Supplementary Table S3. Intercluster separability for all comparisons ($P < 0.0001$) were confirmed. Comparison of grid-wise VP of iAMD eyes versus average grid-wise cluster VP of normal eyes formed the **(B)** overall difference plot, demonstrating significantly decreased VP in iAMD eyes. Color scale at the *bottom*. Further separation by clusters resulted in qualitative and quantitative **(C)** cluster-based difference plots. Corresponding **(D)** box and whisker plots of median differences (%) (fifth and ninety-fifth percentiles) showed greater significance from normal and greater magnitude of decreased VP toward the temporal macula (C_{4-5}) and FAZ (C_6) clusters. *$P < 0.05$, ****$P < 0.0001$. Multiple comparisons between VP of iAMD eyes versus normal eyes at C_{1-6} were performed with Bonferroni adjustment, that is, $P < \frac{0.05}{6}$. Significance values (*red*) denote intercluster comparisons performed with Kruskal-Wallis and Dunn's multiple comparisons tests, that is, $P < 0.0001$ for all intercluster comparisons except C_1 versus C_2 and C_4 versus C_5. C_{1-6}, cluster 1–6 in order of highest to lowest VP.

Investigative Ophthalmology & Visual Science

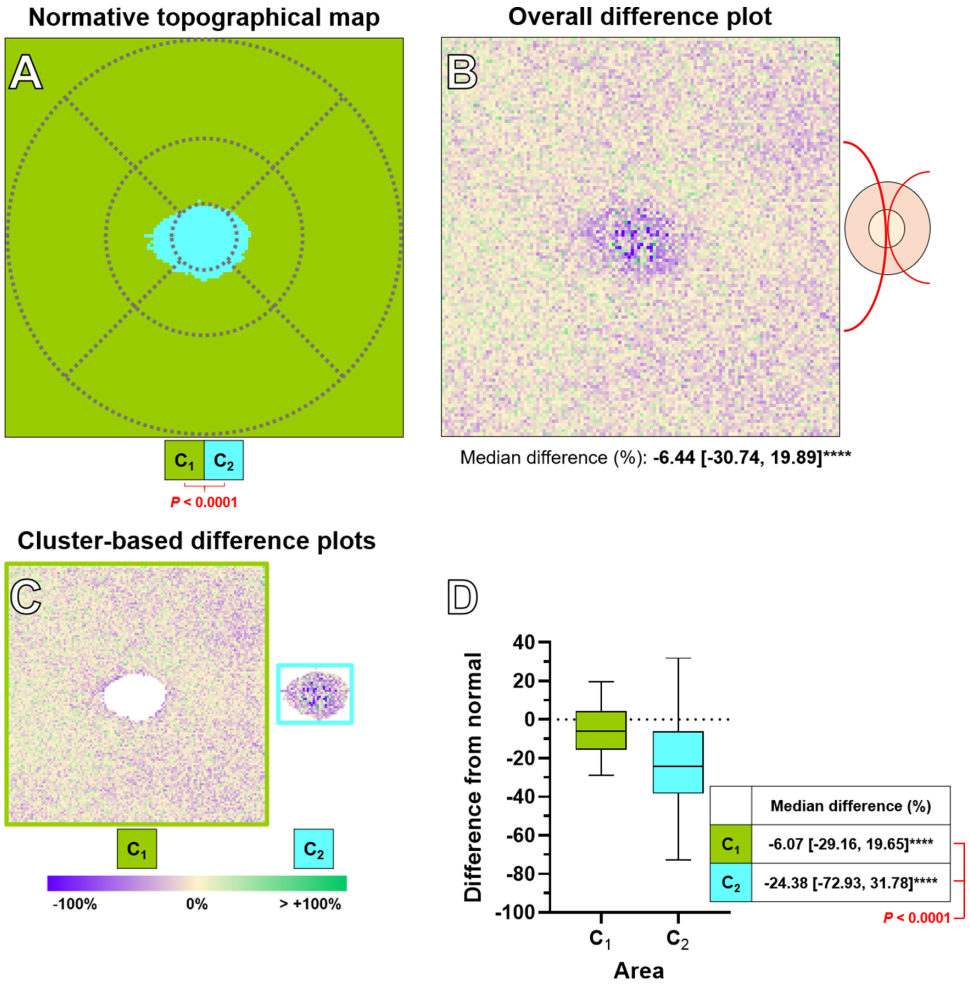

Figure 3. Location-specific analysis: VP difference plots of iAMD eyes compared to normal eyes for the deep vascular complex. Presentation as in Figure 2. **(A)** Normative topographical map of VP in the deep vascular complex [*gray* ETDRS overlay for reference]. **(B)** Overall difference plot, demonstrating significantly decreased VP in iAMD eyes. **(C)** Cluster-based difference plots, and corresponding **(D)** box and whisker plots of median differences (%) (fifth and ninety-fifth percentiles) showed greater magnitude of decreased VP at the FAZ cluster (C_2). ****$P < 0.0001$. Multiple comparisons between VP of iAMD eyes versus normal eyes at $C_{1\text{-}2}$ were performed with Bonferroni adjustment, i.e., $P < \frac{0.05}{2}$. Significance value (*red*) denotes inter-cluster comparison performed with Mann-Whitney *U* test. C_{1-6}, cluster 1–6 in order of highest to lowest VP.

for all method comparisons except global area vs. ETDRS sectors $P < 0.05$; Fig. 5D). There was also significantly less variability using clusters versus a global area versus ETDRS sectors, highlighting improved accuracy using clusters (Brown-Forsythe test, fifth and ninety-fifth percentiles; [−50.58, 23.92] vs. [−57.9, 69.02] vs. [−56.58, 29.77], respectively; $P < 0.0001$; Fig. 5D).

Finally, qualitative analysis of the overall difference plots displayed outcomes that were more consistent in the context of pathophysiological change when using clusters. Specifically, use of a global area and ETDRS sectors exhibited high amounts of increased VP nasally (Fig. 5B, C, *green colored grids*). Use of ETDRS sectors also produced abrupt changes in VP at sector borders (Fig. 5C, *black arrows*). These unusual changes were absent with use of clusters that accounts for actual retinal vascular topography. Location-specific analysis of the deep vascular complex using clusters versus traditional methods were not significantly different (data not shown).

Discussion

This study found significant, location-specific retinal vascular changes in the superficial and deep vascular complex of iAMD eyes compared to normal eyes using high-density en face OCTA cluster analysis. Decreased VP were greater toward the temporal macula and FAZ in the superficial vascular complex, whereas decreased VP were greatest at the FAZ and diffuse elsewhere in the deep vascular complex. These spatial patterns suggest sparing of the RPCP and impairment of the underlying retinal vasculature in iAMD eyes, supporting potential anterograde transsynaptic degeneration as a key pathway in AMD pathophysiology.

OCTA-Derived Normative Topographical Maps Are Representative of Retinal Vascular Anatomy

Development of OCTA-derived normative topographical maps of VP in the superficial and deep vascular complex

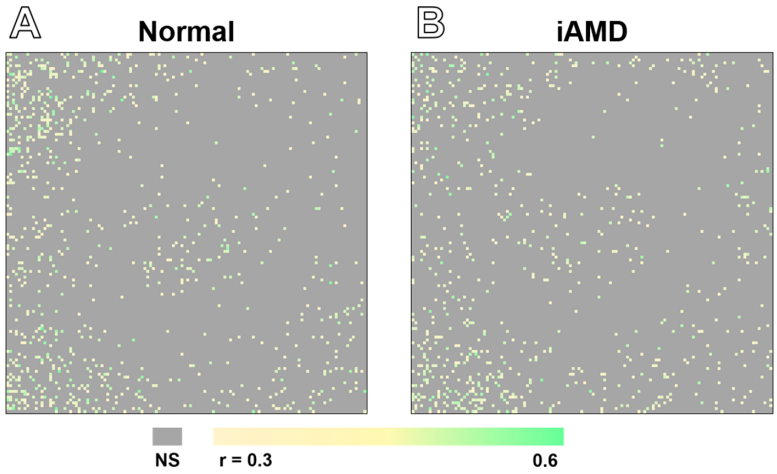

Figure 4. Correlation map between VP in the superficial versus deep vascular complex in **(A)** normal eyes and **(B)** iAMD eyes. All images are in right eye format. Color scale (*bottom*) denotes grids with no statistically significant correlation or weak correlations ($r < 0.3$; NS, *gray*), and grids with statistically significant correlation ($P < 0.05$; *colored*) that were not weak ($r \geq 0.3$). No Spearman's r values were beyond 0.6. Note the moderate correlations at the peripheral macula and perifovea. r, Spearman's rho.

matched the established anatomical profiles of these complexes from histological and OCTA studies.[28,29,37,54–62] Specifically in the superficial vascular complex, nasal clusters represented the RPCP, which has been described as a vascular plexus of radial, nasal distribution that becomes sparse away from the immediate peripapillary zone and then absent at the central macula.[63] It is unlikely that the nasal clusters represent the large retinal arterioles and venules because VP were independent of vessel diameter. The remaining clusters would then represent the underlying SVP, corresponding to approximately the GCL vascular plexus described by Campbell et al.[29] In the deep vascular complex, the majority of the macula area likely represents the ICP and DCP because of their relatively homogeneous configurations within a small portion of the IPL, and the INL and OPL.[28,54]

Location-Specific Analysis Reaffirms Impaired Retinal Vasculature in iAMD

In this study, location-specific analysis found decreased VP in the superficial and deep vascular complex. This was in concordance with a number of previous OCTA studies that have also found decreased vessel density or perfusion in the superficial, deep or both vascular complexes.[12–17,19,24] Some studies, however, suggest no significant changes in either vascular complex in the early stages of AMD.[18,20–23] The disparity in results may be due, in part, to confounders, whereby only some studies controlled for the potential confounding effect of systemic vascular disease[13,14,16,18,20,22] or SSI,[13,19,23] which has significant correlation to OCTA outcomes.[25,26,26,27] Additionally, some studies used unvalidated postimage processing or maintained unprocessed manufacturer software imaging,[18,22] which could affect outcomes because postimage processing has been demonstrated to be a vital step in mitigating noise and improving diagnostic sensitivity and specificity of OCTA imaging.[49,64,65] Our study, however, used strict inclusion criteria that excluded any participants with hypertension, diabetes mellitus, or other significant systemic vascular disease, and any images with SSI below seven. We also performed postimage processing that has been proven to have high reliability and diagnostic sensitivity and specificity.[49] As such, the results from our study present strong evidence supporting other studies that have indicated at least some degree of retinal vascular impairment in early stages of AMD.[12–17,19,24]

An important question to answer is whether evidence of retinal vascular impairment in the early stages of AMD by our study (and others' studies)[12–17,19,24] is clinically significant. Continual improvements in OCTA output signal-to-noise ratio via hardware and software augmentations[66] has meant that there is yet an unsteady concept of a minimal clinically significant effect size.[67–69] Qualitatively, our results emphasize that grouping together the supposed RPCP and underlying vasculature in OCTA analyses is inappropriate, as exampled by the mixed cluster patterns we observed in the superficial vascular complex of normal eyes (temporal-to-nasal with a semblance of concentricity) and also by the contrasting intercluster outcomes in the superficial vascular complex of iAMD eyes. Quantitatively, translation of our results along with other studies will only be clinically applicable once commercial OCTA devices (which produce qualitative or limited quantitative output) adopt more research-proven augmentations. Further study will help amass and refine OCTA augmentations that may help translate significant research findings into clinically usable output.

Cluster-Based Location-Specific Analysis Corroborates Anterograde Transsynaptic Degeneration in iAMD

This study revealed decreased VP toward the temporal macula and FAZ clusters in the superficial vascular complex with relative sparing of VP at the nasal macula in iAMD eyes corresponding to location of the RPCP.[63] Thus our findings suggest relative RPCP sparing in the early stages of AMD, which has some interesting connotations.

Previously, it has been theorized that AMD may emerge as a localized manifestation of systemic disease because of the common inflammatory and vascular pathways AMD shares with systemic comorbidities such as hypertension,

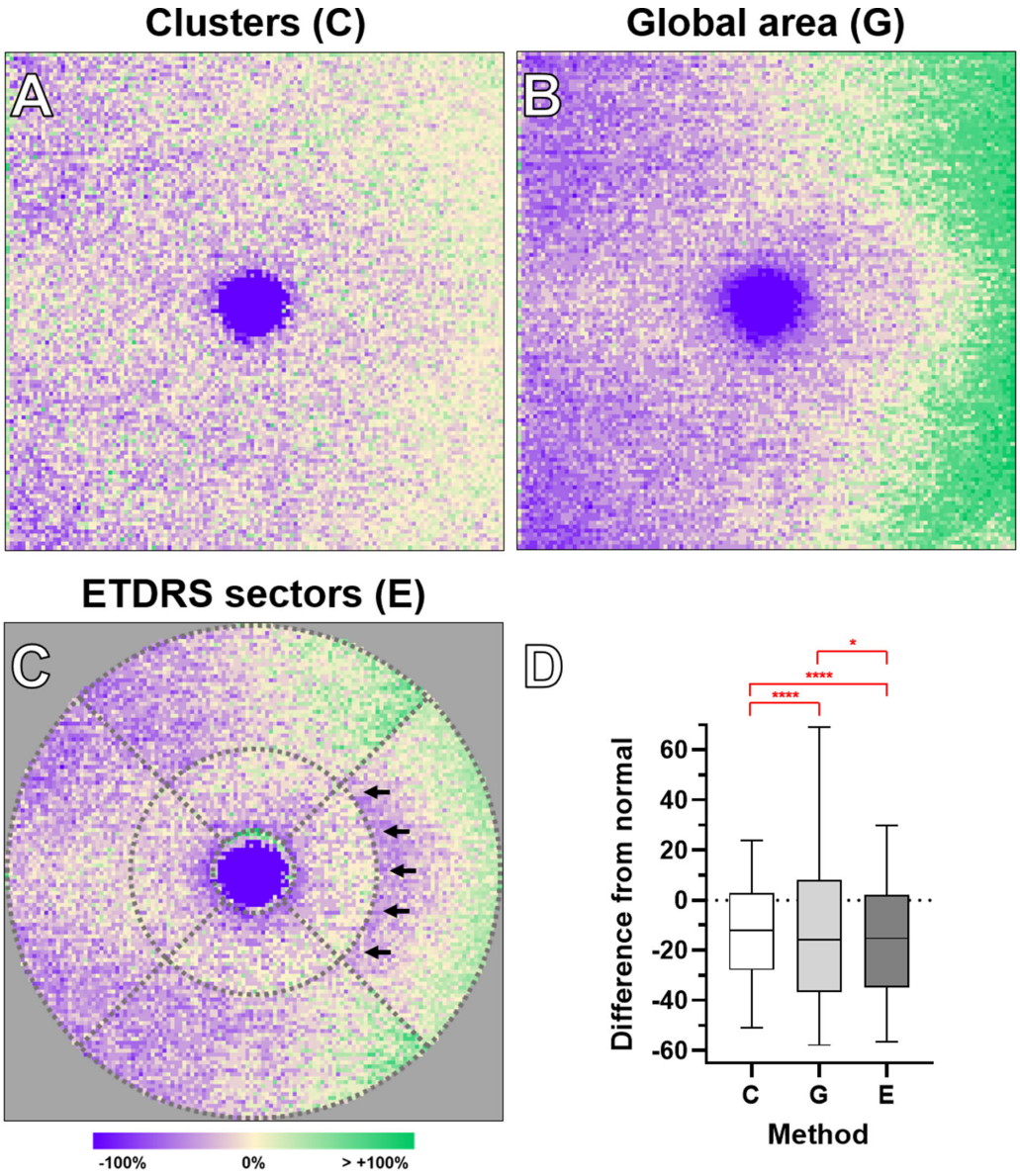

Figure 5. Overall difference plots comparing iAMD eyes to normal eyes in the superficial vascular complex, with normative topography of VP defined using **(A)** clusters, **(B)** a global area, and **(C)** ETDRS sectors. All images are in right eye format. Color scale at the (*bottom*). Qualitatively, note the more consistent outcomes in the context of pathophysiological change when using clusters (**A**), versus the high amounts of increased VP nasally when using a global area and ETDRS sectors (**B, C**), and the abrupt changes in VP at sector borders using ETDRS sectors (**C**, *black arrows*). **(D)** Quantitative box and whisker plots of median differences (%) [fifth and ninety-fifth percentiles] using the three methods, highlighting significantly less variability associated with use of clusters versus a global area versus ETDRS sectors. Significance values (*red*) denote inter-method comparisons performed with Kruskal-Wallis and Dunn's multiple comparisons tests. $^{*}P < 0.05$, $^{****}P < 0.0001$. C, clusters; G, global area; E, early treatment for diabetic retinopathy study sectors.

dyslipidemia, and coronary heart disease.[70,71] Indeed, there is evidence linking extraocular vascular impairment[3–7] and systemic disease particularly of a vascular nature[72–76] to the presence of AMD. Our results showed sparing of the RPCP that controverts this systemic pathophysiological model of AMD. The RPCP shares a common source, that is, the ophthalmic artery, with other retinal vascular plexuses that otherwise demonstrated vascular impairment in this study. Thus, if retinal vascular impairment in iAMD were a direct consequence of systemic vascular impairment, we would expect a generalized spatial pattern of vascular loss in all areas of the superficial and deep vascular complex. This study is not the first to present evidence challenging this model, because not all diagnoses of iAMD are accompanied by extraocular/systemic vascular impairment.

Alternatively, Feigl et al.[77] have proposed that AMD involves primary, localized insult at the outer retina or choroid that then propagates anterograde to involve the inner retina as well—known as anterograde transsynaptic degeneration.[78] This model is reflected in the spatial patterns of retinal vascular impairment that we observed, being relatively diffuse in the deep vascular complex and partial in the superficial vascular complex. The observed

sparing of the RPCP possibly suggests that chronologically, the anterograde degeneration may not yet have reached the most superficial portion of the retinal vasculature. In following this line of reasoning, our results suggest that primary insult in the early stages of AMD is more likely to be at the outer retina rather than the choroidal vasculature. The choroid is also commonly supplied by the ophthalmic artery, and thus we would also expect RPCP impairment if primary insult in the early stages of AMD were vascular in nature. Corroborative evidence for this theory may be seen in histological studies demonstrating partial choroidal degeneration underlying areas of complete retinal pigment epithelium atrophy, suggesting the latter to be the primary event.[79,80] Similarly, Toto et al.[16] have reported choroidal vascular change at the intermediate but not early stage of AMD, suggesting vascular change to be secondary to outer retinal insult. Future studies involving longitudinal, location-specific examination of the retinal vasculature in the early stages of AMD eyes are needed to confirm the chronology of events.

These two aforementioned models of AMD pathogenesis may be further complicated by the involvement of astrocytes, located principally around the RPCP. Astrocytes in the brain have demonstrated neurovascular coupling,[81] whereby interaction of adjacent neurons and vasculature maintains homeostasis. Similarly, recent studies have suggested that retinal glial cells also propagate signaling to enable neurovascular coupling in the retina.[82] In conjunction with astrocytes' neurotrophic and mechanical support of retinal nerve fibres,[82] astrocytes may then also provide a preservatory mechanism for the RPCP in disease. The exact role of astrocytes and other glial cells in maintaining retinal vascular integrity, however, is still being explored.

Further Evidence of Interconnectivity Between the Superficial and Deep Vascular Complex

OCTA en face imaging by nature is contingent on adequate signal penetration through the superficial vascular complex before it reaches the deep vascular complex. To determine whether there was a possibility that outcomes in the deep vascular complex were shaped by outcomes in the superficial vascular complex, we correlated grid-wise VP between the two complexes in normal and iAMD eyes. Correlational maps were in concordance with anatomical data, showing moderate correlations between the superficial and deep vascular complex in normal and iAMD eyes at areas where the vascular plexuses converge, such as toward the peripheral macula and perifoveal capillary ring.[29,83] This was likely exacerbated by use of OCTA manufacturer software that constrains segmentation of whole slab borders without consideration for vascular plexus convergence. Moderate correlations between the two vascular complexes in the temporal macula may also explain the subtly lesser magnitude of decreased VP toward the temporal macula in the deep vascular complex, because decreased VP in the superficial vascular complex may "reveal" more of the underlying deep retinal vasculature caused by greater signal penetrance. Therefore future studies using en face OCTA analyses will need to be cautious regarding interpretations of the deeper retinal or even choroidal vascular plexuses.

Location-Specific Analysis Using Clusters Provides More Consistent Outcomes Relative to Traditional Methods

We found that high-density en face OCTA analysis using clusters produced an overall difference plot that was more consistent in the context of iAMD pathophysiology, in contrast to the unusual high amounts of increased VP nasally when using global area and ETDRS sectors and also in contrast to the abrupt changes in VP at sector borders using ETDRS sectors. The use of clusters was also associated with less variability than traditional methods, highlighting the reliability of location-specific analysis using clusters. This was consistent with previous findings that clusters more accurately reflect retinal anatomy compared to traditional methods such as using the ETDRS sectors.[34] Similarly, future OCTA analyses will need to appropriately account for normative retinal vascular topography to avoid anomalous outcomes such as those demonstrated in our comparison of location-specific analysis methods.

Limitations

This study was associated with some limitations. Primarily, we used cross-sectional data, which enables only inferences of the pathophysiological changes and their temporal relationships within iAMD. In this study, only iAMD was considered because we hypothesized that the level of location-specific retinal vascular changes in the early stages of AMD would positively correlate with disease severity. Thus detecting this change would have been most probable at the intermediate rather than early stage of AMD. Future longitudinal, location-specific OCTA examination of the retinal vasculature in early and iAMD eyes may be able to confirm a timeline of events. Similarly, our high-density en face OCTA cluster analysis was applied to a cohort of iAMD participants as assigned on the basis of the Beckman Initiative classification scheme,[40] meaning that participants may have had varying extents of drusen, pigmentary abnormalities, or nongeographic atrophy. Further study is underway to examine relationships between location-specific retinal vascular changes in iAMD and specific iAMD phenotypes.

Conclusions

Location-specific retinal vascular changes in the superficial and deep vascular complex of iAMD eyes compared to normal eyes were evident using age-matched, high-density en face OCTA cluster analysis. Specifically, VP changes in iAMD eyes suggests relative sparing of the RPCP and impairment of the underlying retinal vasculature, supporting potential anterograde transsynaptic degeneration rather than systemic causes of inner retinal changes in iAMD. These results provide location-specific data regarding iAMD vascular impairment to better guide future diagnostic and management protocol.

Acknowledgments

The authors thank Gordon Doig (Centre for Eye Health, Sydney, Australia) for methodological and writing advice.

Supported by research grants from the Rebecca Cooper Foundation and the National Health and Medical Research Council of

Australia (NHMRC Grant no. 1174385), the Australian Research Training Program scholarship, and Guide Dogs NSW/ACT.

Disclosure: **M. Trinh,** None; **M. Kalloniatis,** None; **L. Nivison-Smith,** None

References

1. Wong WL, Su X, Li X, et al. Global prevalence of age-related macular degeneration and disease burden projection for 2020 and 2040: a systematic review and meta-analysis. *Lancet Global Health*. 2014;2:e106–e116.
2. Ambati J, Ambati BK, Yoo SH, Ianchulev S, Adamis AP. Age-related macular degeneration: etiology, pathogenesis, and therapeutic strategies. *Surv Ophthalmol*. 2003;48:257–293.
3. Hosal BM, Karakoç G, Gürsel E, Camur M. Color Doppler imaging of the retrobulbar circulation in age-related macular degeneration. *Eur J Ophthalmol*. 1998;8:234–238.
4. Ciulla TA, Harris A, Chung HS, et al. Color Doppler imaging discloses reduced ocular blood flow velocities in nonexudative age-related macular degeneration. *Am J Ophthalmol*. 1999;128:75–80.
5. Friedman E, Krupsky S, Lane AM, et al. Ocular blood flow velocity in age-related macular degeneration. *Ophthalmology*. 1995;102:640–646.
6. Dimitrova G, Tamaki Y, Kato S. Retrobulbar circulation in patients with age-related maculopathy. *Eye; London*. 2002;16:580–586.
7. Sato E, Feke GT, Menke MN, Wallace McMeel J. Retinal haemodynamics in patients with age-related macular degeneration. *Eye*. 2006;20:697–702.
8. Kornzweig AL, Eliasoph I, Feldstein M. The Retinal Vasculature in Macular Degeneration. *Arch Ophthalmol*. 1966;75:326–333.
9. Wang JJ. Retinal vessel wall signs and the 5 year incidence of age related maculopathy: the Blue Mountains Eye Study. *Br J Ophthalmol*. 2004;88:104–109.
10. Lutty GA, McLeod DS, Bhutto IA, Edwards MM, Seddon JM. Choriocapillaris dropout in early age-related macular degeneration. *Exp Eye Res*. 2020;192:107939.
11. Biesemeier A, Taubitz T, Julien S, Yoeruek E, Schraermeyer U. Choriocapillaris breakdown precedes retinal degeneration in age-related macular degeneration. *Neurobiol Aging*. 2014;35:2562–2573.
12. Lee B, Ahn J, Yun C, Kim S, Oh J. Variation of Retinal and Choroidal Vasculatures in Patients With Age-Related Macular Degeneration. *Invest Ophthalmol Vis Sci*. 2018;59:5246–5255.
13. Ozcaliskan S, Artunay O, Balci S, Perente I, Yenerel NM. Quantitative analysis of inner retinal structural and microvascular alterations in intermediate age-related macular degeneration: a swept-source OCT angiography study. *Photodiagnosis Photodynamic Ther*. 2020;32:102030.
14. Shin Y-I, Kim JM, Lee M-W, Jo Y-J, Kim J-Y. Characteristics of the foveal microvasculature in Asian patients with dry age-related macular degeneration: an optical coherence tomography angiography study. *OPH*. 2020;243:145–153.
15. Toto L, Borrelli E, Di Antonio L, Carpineto P, Mastropasqua R. Retinal vascular plexuses' changes in dry age-related macular degeneration, evaluated by means of optical coherence tomography angiography. *Retina*. 2016;36:1566–1572.
16. Toto L, Borrelli E, Mastropasqua R, et al. Association between outer retinal alterations and microvascular changes in intermediate stage age-related macular degeneration: an optical coherence tomography angiography study. *Br J Ophthalmol*. 2017;101:774–779.
17. Trinh M, Kalloniatis M, Nivison-Smith L. Vascular changes in intermediate age-related macular degeneration quantified using optical coherence tomography angiography. *Trans Vis Sci Tech*. 2019;8:20–20.
18. Vaghefi E, Hill S, Kersten HM, Squirrell D. Quantification of optical coherence tomography angiography in age and age-related macular degeneration using vessel density analysis. *Asia Pac J Ophthalmol (Phila)*. 2020;9:137–143.
19. Cicinelli MV, Rabiolo A, Sacconi R, et al. Optical coherence tomography angiography in dry age-related macular degeneration. *Surv Ophthalmol*. 2018;63:236–244.
20. Ahn SM, Lee SY, Hwang SY, et al. Retinal vascular flow and choroidal thickness in eyes with early age-related macular degeneration with reticular pseudodrusen. *BMC Ophthalmol*. 2018;18:184.
21. Lee SC, Tran S, Amin A, et al. Retinal vessel density in exudative and nonexudative age-related macular degeneration on optical coherence tomography angiography. *American Journal of Ophthalmology*. 2020;212:7–16.
22. Parisi V, Ziccardi L, Costanzo E, et al. Macular functional and morphological changes in intermediate age-related maculopathy. *Invest Ophthalmol Vis Sci*. 2020;61:11–11.
23. Reiter GS, Told R, Schlanitz FG, et al. Longitudinal association between drusen volume and retinal capillary perfusion in intermediate age-related macular degeneration. *Invest Ophthalmol Vis Sci*. 2019;60:2503–2508.
24. Cicinelli MV, Rabiolo A, Sacconi R, et al. Retinal vascular alterations in reticular pseudodrusen with and without outer retinal atrophy assessed by optical coherence tomography angiography. *Br J Ophthalmol*. 2018;102:1192–1198.
25. Lim HB, Kim YW, Kim JM, Jo YJ, Kim JY. The importance of signal strength in quantitative assessment of retinal vessel density using optical coherence tomography angiography. *Sci Rep*. 2018;8:12897.
26. Yu JJ, Camino A, Liu L, et al. Signal strength reduction effects in OCT angiography. *Ophthalmol Retina* 2019;3:835–842.
27. Czakó C, István L, Benyó F, et al. The impact of deterministic signal loss on oct angiography measurements. *Trans Vis Sci Tech*. 2020;9:10–10.
28. Tan PEZ, Paula KY, Balaratnasingam C, et al. Quantitative confocal imaging of the retinal microvasculature in the human retina. *Invest Ophthalmol Vis Sci*. 2012;53:5728–5736.
29. Campbell JP, Zhang M, Hwang TS, et al. Detailed vascular anatomy of the human retina by projection-resolved optical coherence tomography angiography. *Sci Rep*. 2017;7:42201.
30. Choi AYJ, Nivison-Smith L, Phu J, et al. Contrast sensitivity isocontours of the central visual field. *Sci Rep*. 2019;9:1–14.
31. Tong J, Phu J, Khuu SK, et al. Development of a spatial model of age-related change in the macular ganglion cell layer to predict function from structural changes. *Am J Ophthalmol*. 2019;208:166–177.
32. Yoshioka N, Zangerl B, Nivison-Smith L, et al. Pattern recognition analysis of age-related retinal ganglion cell signatures in the human eye. *Invest Ophthalmol Vis Sci*. 2017;58:3086–3099.
33. Yoshioka N, Zangerl B, Phu J, et al. Consistency of structure-function correlation between spatially scaled visual field stimuli and in vivo OCT ganglion cell counts. *Invest Ophthalmol Vis Sci*. 2018;59:1693–1703.
34. Trinh M, Khou V, Zangerl B, Kalloniatis M, Nivison-Smith L. Modelling normal age-related changes in individual retinal layers using location-specific OCT analysis. *Sci Rep*. 2021;11:558.
35. Wang H, Kalloniatis M. Clinical outcomes of the Centre for Eye Health: an intra-professional optometry-led collaborative eye care clinic in Australia. *Clin Exp Optom*. 2021;0:1–10.

Investigative Ophthalmology & Visual Science

36. Wei Y, Jiang H, Shi Y,et al. Age-related alterations in the retinal microvasculature, microcirculation, and microstructure. *Invest Ophthalmol Vis Sci*. 2017;58:3804–3817.
37. Garrity ST, Iafe NA, Phasukkijwatana N, Chen X, Sarraf D. Quantitative analysis of three distinct retinal capillary plexuses in healthy eyes using optical coherence tomography angiography. *Invest Ophthalmol Vis Sci*. 2017;58:5548–5555.
38. Iafe NA, Phasukkijwatana N, Chen X, Sarraf D. Retinal capillary density and foveal avascular zone area are age-dependent: quantitative analysis using optical coherence tomography angiography. *Invest Ophthalmol Vis Sci*. 2016;57:5780–5787.
39. Kraker JA, Omoba BS, Cava JA, et al. Assessing the influence of OCT-A device and scan size on retinal vascular metrics. *Trans Vis Sci Tech*. 2020;9:7–7.
40. Ferris FL, III, Wilkinson CP, Bird A, et al. Clinical classification of age-related macular degeneration. *Ophthalmology*. 2013;120:844–851.
41. Sleiman K, Veerappan M, Winter KP, et al. Optical coherence tomography predictors of risk for progression to non-neovascular atrophic age-related macular degeneration. *Ophthalmology*. 2017;124:1764–1777.
42. Hallak JA, de Sisternes L, Osborne A, et al. Imaging, genetic, and demographic factors associated with conversion to neovascular age-related macular degeneration: secondary analysis of a randomized clinical trial. *JAMA Ophthalmol*. 2019;137:738–744.
43. Waldstein SM, Vogl WD, Bogunovic H, et al. Characterization of drusen and hyperreflective foci as biomarkers for disease progression in age-related macular degeneration using artificial intelligence in optical coherence tomography. *JAMA Ophthalmol*. 2020;138:740–747.
44. Guymer RH, Baird PN, Varsamidis M, et al. Proof of concept, randomized, placebo-controlled study of the effect of simvastatin on the course of age-related macular degeneration. *PLoS One*. 2013;8(12):e83759.
45. Rao HL, Pradhan ZS, Weinreb RN, et al. Determinants of peripapillary and macular vessel densities measured by optical coherence tomography angiography in normal eyes. *J Glaucoma* 2017;26:491–497.
46. Wang J, Jiang J, Zhang Y, et al. Retinal and choroidal vascular changes in coronary heart disease: an optical coherence tomography angiography study. *Biomed Opt Express*. 2019;10:1532–1544.
47. Çiloğlu E, Unal F, Sukgen E, Koçluk Y, Dogan N. Evaluation of foveal avascular zone and capillary plexus in smokers using optical coherence tomography angiography. *J Curr Ophthalmol*. 20;32:53–57.
48. Leung H, Wang JJ, Rochtchina E, et al. Dyslipidaemia and microvascular disease in the retina. *Eye (Lond)*. 2005;19:861–868.
49. Rabiolo A, Gelormini F, Sacconi R, et al. Comparison of methods to quantify macular and peripapillary vessel density in optical coherence tomography angiography. *PLoS One*. 2018;13:e0205773.
50. Bell MA, Ball MJ. Morphometric comparison of hippocampal microvasculature in ageing and demented people: diameters and densities. *Acta Neuropathol*. 1981;53:299–318.
51. Gelbard R, Goldman O, Spiegler I. Investigating diversity of clustering methods: An empirical comparison. *Data Knowl Eng*. 2007;63:155–166.
52. Macmillan N, Creelman D. *Detection Theory: A User's Guide. Detection Theory: A User's Guide:* 2nd edition Vol. xix. New York: Psychology Press; 2004.
53. Derksen S, Keselman HJ. Backward, forward and stepwise automated subset selection algorithms: Frequency of obtaining authentic and noise variables. *Br J Math Stat Psychol*. 1992;45:265–282.
54. Chan G, Balaratnasingam C, Paula KY, et al. Quantitative morphometry of perifoveal capillary networks in the human retina. *Invest Ophthalmol Vis Sci*. 2012;53:5502–5514.
55. Lavia C, Bonnin S, Maule M, Erginay A, Tadayoni R, Gaudric A. Vessel density of superficial, intermediate, and deep capillary plexuses using optical coherence tomography angiography. *Retina* 2019;39:247–258.
56. Hashmani N, Hashmani S, Murad A, Baig N. Macular vascular density at the superficial capillary plexus using the optical coherence tomography angiography. *Clin Ophthalmol*. 2019;13:295–302.
57. Tan PEZ, Balaratnasingam C, Xu J, et al. Quantitative comparison of retinal capillary images derived by speckle variance optical coherence tomography with histology. *Invest Ophthalmol Vis Sci*. 2015;56:3989–3996.
58. Chan G, Balaratnasingam C, Xu J, et al. In vivo optical imaging of human retinal capillary networks using speckle variance optical coherence tomography with quantitative clinico-histological correlation. *Microvasc Res*. 2015;100:32–39.
59. Muraoka Y, Uji A, Ishikura M, Iida Y, Ooto S, Tsujikawa A. Segmentation of the four-layered retinal vasculature using high-resolution optical coherence tomography angiography reveals the microcirculation unit. *Invest Ophthalmol Vis Sci*. 2018;59:5847–5853.
60. Onishi AC, Nesper PL, Roberts PK, et al. Importance of considering the middle capillary plexus on OCT angiography in diabetic retinopathy. *Invest Ophthalmol Vis Sci*. 2018;59:2167–2176.
61. Park J, Soetikno B, Fawzi A. Characterization of the middle capillary plexus using optical coherence tomography angiography in healthy and diabetic eyes. *Retina*. 2016;36:2039–2050.
62. Freund KB, Gattoussi S, Leong BCS. Dense B-scan optical coherence tomography angiography. *Am J Ophthalmol*. 2018;190:78–88.
63. Cuenca N, Ortuño-Lizarán I, Sánchez-Sáez X, et al. Interpretation of OCT and OCTA images from a histological approach: clinical and experimental implications. *Prog Retin Eye Res*. 2020;77:100828.
64. Cole ED, Moult EM, Dang S, et al. The definition, rationale, and effects of thresholding in OCT angiography. *Ophthalmol Retina*. 2017;1:435–447.
65. Terheyden JH, Wintergerst MW, Falahat P, Berger M, Holz FG, Finger RP. Automated thresholding algorithms outperform manual thresholding in macular optical coherence tomography angiography image analysis. *PLoS One*. 2020;15:e0230260.
66. Borrelli E, Sadda SR, Uji A, Querques G. Pearls and pitfalls of optical coherence tomography angiography imaging: a review. *Ophthalmol Ther*. 2019;8:215–226.
67. Jaeschke R, Singer J, Guyatt GH. Measurement of health status: ascertaining the minimal clinically important difference. *Control Clin Trials*. 1989;10:407–415.
68. Keefe RSE, Kraemer HC, Epstein RS, et al. Defining a clinically meaningful effect for the design and interpretation of randomized controlled trials. *Innov Clin Neurosci*. 2013;10:4S–19S.
69. Sullivan GM, Feinn R. Using effect size—or why the P value is not enough. *J Grad Med Educ*. 2012;4:279–282.
70. Cheung CMG, Wong TY. Is age-related macular degeneration a manifestation of systemic disease? New prospects for early intervention and treatment. *J Intern Med*. 2014;276:140–153.
71. Feigl B. Age-related maculopathy in the light of ischaemia. *Clin Exp Optom*. 2007;90:263–271.
72. Clemons TE, Milton RC, Klein R, Seddon JM, Ferris FL, 3rd. Risk factors for the incidence of Advanced

Investigative Ophthalmology & Visual Science

Age-Related Macular Degeneration in the Age-Related Eye Disease Study (AREDS) AREDS report no. 19. *Ophthalmology*. 2005;112:533–539.

73. Klein R, Klein BE, Knudtson MD, et al. Subclinical atherosclerotic cardiovascular disease and early age-related macular degeneration in a multiracial cohort: the multiethnic study of atherosclerosis. *Arch Ophthalmol*. 2007;125:534–543.
74. Hyman L, Schachat AP, He Q, Leske MC. Hypertension, cardiovascular disease, and age-related macular degeneration. Age-Related Macular Degeneration Risk Factors Study Group. *Arch Ophthalmol*. 2000;118:351–358.
75. Mares-Perlman JA, Brady WE, Klein R, VandenLangenberg GM, Klein BE, Palta M. Dietary fat and age-related maculopathy. *Arch Ophthalmol*. 1995;113:743–748.
76. Vingerling JR, Dielemans I, Bots ML, Hofman A, Grobbee DE, de Jong PT. Age-related macular degeneration is associated with atherosclerosis. The Rotterdam Study. *Am J Epidemiol*. 1995;142:404–409.
77. Feigl B, Brown B, Lovie-Kitchin J, Swann P. Functional loss in early age-related maculopathy: the ischaemia postreceptoral hypothesis. *Eye*. 2007;21:689–696.
78. Panneman EL, Coric D, Tran LMD, de Vries-Knoppert WAEJ, Petzold A. Progression of anterograde trans-synaptic degeneration in the human retina is modulated by axonal convergence and divergence. *Neuroophthalmology*. 2019;43:382–390.
79. McLeod DS, Grebe R, Bhutto I, Merges C, Baba T, Lutty GA. Relationship between RPE and choriocapillaris in age-related macular degeneration. *Invest Ophthalmol Vis Sci*. 2009;50:4982–4991.
80. Korte GE, Reppucci V, Henkind P. RPE destruction causes choriocapillary atrophy. *Invest Ophthalmol Vis Sci*. 1984;25:1135–1145.
81. Attwell D, Buchan AM, Charpak S, Lauritzen M, MacVicar BA, Newman EA. Glial and neuronal control of brain blood flow. *Nature*. 2010;468:232–243.
82. Vecino E, Rodriguez FD, Ruzafa N, Pereiro X, Sharma SC. Glia–neuron interactions in the mammalian retina. *Progr Retinal Eye Res*. 2016;51:1–40.
83. Spaide RF, Fujimoto JG, Waheed NK, Sadda SR, Staurenghi G. Optical coherence tomography angiography. *Prog Retin Eye Res*. 2018;64:1–55.

Investigative Ophthalmology & Visual Science